Overview

Phosphorene: what can we know from computations?

Yu Jing,[1,2,3,4,5,6] Xu Zhang[1,2,3,4,5,6] and Zhen Zhou[1,2,3,4,5,6]*

The past year has witnessed the fast growth of investigations on monolayer and few-layer black phosphorous, termed as 'phosphorene.' The intrinsic mechanical, electronic, thermal, and optical properties of phosphorene, which have mainly been revealed by computations, endow it with significant potential applications to the fields of electronics, optoelectronics, thermoelectrics, catalysis, and energy storage. In this overview, we summarize the computational investigations on phosphorene from aspects of inherent quality, properties, potential applications, and new allotropes, and manage to interpret what we can know about phosphorene from computations. We hope that this overview would help better understand phosphorene and provide guidance for experimental and computational colleagues to further investigate phosphorene and other novel two-dimensional materials.

How to cite this article:
WIREs Comput Mol Sci 2016, 6:5–19. doi: 10.1002/wcms.1234

INTRODUCTION

Located in the third period and the VA group, phosphorus is a familiar element abundant in the earth's crust. There are two common morphologies of phosphorus, white phosphorus and red phosphorus, both of which are easy to be ignited by fire. As the third morphology of phosphorus, black phosphorus is more chemically stable and ignition resistant than the red and white ones. Black phosphorus also shows advantages in effective electron and heat conductance over white and red phosphorus.[1] However, the most attractive property of black phosphorus is its layered structure. Stacked by the surmountable van der Waals (vdW) interactions, black phosphorus in the orthorhombic crystallization with space group cmca,[2] is supposed to be potentially exfoliated into individual atomic layers, which are named as 'phosphorene.' In fact, black phosphorus has been known for a century before it was exfoliated into phosphorene. Composed of only one element, two-dimensional (2D) phosphorene is expected to exhibit fantastic properties akin to graphene and duplicate the success of 2D materials in wide applications.

In the past year, great efforts have been devoted to seeking effective methods to prepare phosphorene.[3,4] Up to now, monolayer or few-layer phosphorene have been experimentally realized via Scotch tape-based mechanical exfoliation,[5,6] liquid exfoliation under bath ultrasonication,[7] and Ar^+ plasma thinning process before mechanical cleavage.[8] After the experimental realization, more research interest was stimulated to study the intrinsic properties of phosphorene. Actually, even long before the experimental exfoliation of black phosphorous, theoretical researchers had already probed the properties of phosphorene.

*Correspondence to: zhouzhen@nankai.edu.cn

[1]Key Laboratory of Advanced Energy Materials Chemistry (Ministry of Education), Nankai University, Tianjin, P. R. China

[2]Computational Centre for Molecular Science, Nankai University, Tianjin, P. R. China

[3]Institute of New Energy Material Chemistry, Nankai University, Tianjin, P. R. China

[4]Collaborative Innovation Center of Chemical Science and Engineering (Tianjin), Nankai University, Tianjin, P. R. China

[5]School of Materials Science and Engineering, Nankai University, Tianjin, P. R. China

[6]National Institute for Advanced Materials, Nankai University, Tianjin, P. R. China

Conflict of interest: The authors have declared no conflicts of interest for this article.

Thirty years ago, Morita et al. noticed the single puckered black phosphorus layer (namely phosphorene) and investigated the band structure of phosphorene through tight-binding computations,[9,10] and they found that phosphorene is semiconducting with a direct band gap of ~2.5 eV, which was highly consistent with the recent experimental results. Since last year, abundant computations with higher accuracy than the tight-binding method have been widely performed to investigate the structural configurations, intrinsic properties, and possible applications of phosphorene. An overview of those computational studies on phosphorene is urgent to better trace the emergency and development of phosphorene in computational materials science. Meanwhile, good comprehension of how computations investigate phosphorene can also facilitate the theoretical explorations of other new materials.

In this overview, the recent computational studies on phosphorene are summarized. After the structural configurations and intrinsic properties of phosphorene are briefly introduced, different computational methodologies, especially the selected functional on predicting the structure and properties of phosphorene, are compared. Various processes in tuning the properties of phosphorene are then summarized, including applying elastic strain and vertical electric field, cutting phosphorene into nanoribbons, stacking phosphorene monolayers with different orders, and surface doping with atoms and molecules. We also present a generalization on the possible applications of phosphorene to electronics and energy storage from the theoretical side. Finally, computational insights are interpreted into predicting possible allotropes of phosphorene.

STRUCTURE AND PROPERTIES

Two-dimensional Configuration of Black Phosphorene

As shown in Figure 1(a), monolayer phosphorene consists of two atomic layers of P atoms that are arranged in a puckered honeycomb lattice described by C_{2h} point group. Different from hexagonal graphene, phosphorene has an orthogonal unit cell and exhibits armchair and zigzag configuration along the x and y direction, respectively, resulting in a remarkable structure anisotropy. The intralayer bonding in phosphorene is dominated by the sp^3 hybridized P atoms, resulting in three bonding orbitals per two atoms augmented by lone pairs associated with each atom. By testing the accuracy of different functionals of density functional theory (DFT) in simulating the geometric structure of black phosphorous, Qiao et al. proposed that PBE-G06 and optB86b-vdW functional can give the best results in describing the structure of phosphorene.[11] Here, both PBE-G06 and optB86b-vdW functional can correctly describe the weak interactions between phosphorene layers, which are based on the semi-empirical potential (DFT-D) and nonlocal correlation functional (vdW-DF), respectively.[12] As DFT-D treats the dispersion interactions semi-empirically, it is less expensive than vdW-DF. Nevertheless, the optB86b-vdW method can generally give smaller errors in optimizing geometry than other functionals (optB88-vdW, revPBEvdW, rPW86-vdW2, etc.) and can be adapted to wider applications.[13] For the lattice optimization of phosphorene, different DFT methods as presented in Table 1 predict the lattice parameters with discrepancy lower than 2.6% in the x and 1.5% in

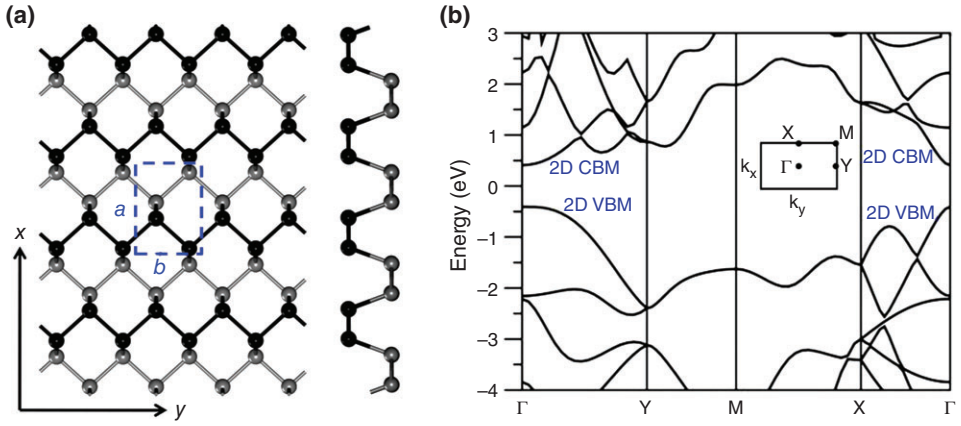

FIGURE 1 | (a) Structure schematic of two-dimensional (2D) phosphorene in the top (left) and side (right) views. The unit cell is labeled in dashed blue lines; (b) DFT band structure of 2D phosphorene and the corresponding Brillouin zone. (Reproduced with permission from Ref 20 Copyright 2014 American Chemical Society)

TABLE 1 | Computed Lattice Parameters and Band Gaps of Phosphorene based on Different Methods in Comparison with the Experimental Results

Method	Lattice *a* (Å)	Lattice *b* (Å)	Band Gap (eV)	Refs.
PBE	4.627	3.298	0.92	Peng[40]; Sa[22]
optB88_vdW	4.506	3.303	0.76	Sa[22]
HSE06@PBE	4.627	3.298	1.54	Sa[22]
HSE06@optB88_vdW	4.58	3.32	1.51	Qiao[11]
LDA_mBJ@optB88_vdW	4.58	3.32	1.41	Qiao[11]
ModifiedHSE06@PBE	4.62	3.35	1.0	Liu[6]
G_0W_0@PBE	4.627	3.298	2.08	Sa[22]
GW_0@PBE	4.52	3.31	1.94	Liang[20]
G_0W_0@PBE_vdW	—	—	2.0	Tran[19]
BSE(G_0W_0/G_1W_1)	—	—	1.2/1.4	Tran[19]
GW	—	—	1.60	Rudenko[31]
Measured PL spectra	—	—	1.45	Liu[6]
Surface STM detection	—	—	2.1	Liang[20]

PL, photoluminescence; STM, scanning tunneling microscopy.

y direction; therefore, the effect of induced strain could be neglected. For example, the Perdew, Burke, and Ernzerhof (PBE) computations indicate that the lattice parameters of phosphorene are 4.627 and 3.298 Å for *a* and *b*, respectively, and the optB88-vdW computations indicate that phosphorene has the lattice parameters of 4.58 Å for *a* and 3.32 Å for *b*. The anisotropic structural properties of phosphorene also endow it with anisotropic mechanical, electronic, optical, and thermal properties, which will be introduced in the following sections.

Mechanical Properties

The unique structural properties of phosphorene firstly endow it with special mechanical properties. DFT–PBE computations by Jiang et al. demonstrated that the Young's modulus of phosphorene is anisotropic.[14] Specifically, the in-plane Young's modulus for phosphorene are 44 and 166 GPa along the *x* and *y* direction, respectively, indicating that the puckered *x* direction is more ductile than the *y* direction. Wei et al. demonstrated computationally that phosphorene monolayer can endure tensile strain up to 30 and 27% in the *x* and *y* direction, respectively.[15] The more pronounced flexibility in the *x* direction can be attributed to the stretchable pucker of phosphorene in this direction. Remarkably, the puckered structure leads to a negative Poisson's ratio of phosphorene, which makes it significantly distinctive from other 2D materials.[16] Via *ab initio* computations, Jiang et al. revealed that the pucker of phosphorene can function as a nanoscale re-entrant structure and introduce a negative Poisson's ratio in the out-of-plane direction during the deformation of phosphorene in its *y* direction. This fantastic mechanical property renders phosphorene an attractive 2D auxetic material. Since previous DFT-D results on the pressure coefficient and elastic constants of bulk black phosphorus are in good agreement with experimental values,[17] the mechanical properties of phosphorene predicted by DFT computations are reliable.

Electronic Properties

As a new mono-element 2D crystal, what novel electronic properties can phosphorene present? To address this issue, many theoretical studies have been conducted to investigate the electronic properties of phosphorene. It is known that DFT usually underestimates the band gap of semiconductors, while GW method is more reliable in determining an accurate band gap for semiconductors. The GW method is based on the Green's function (G) and screened Coulomb interaction (W). It can accurately describe ground and excited states of materials, and is superior to DFT that can only deal with the ground state. Based on the local-density approximation (LDA)/generalized gradient approximation (GGA) single-particle Hamiltonian H_0, G_0W_0 is successful in computing the band gap of materials, especially semiconductors and insulators composed of light elements.[18] By using G_0W_0 method, Tran et al. predicted a band gap of ~2.0 eV for phosphorene.[19] Very recently, scanning tunneling microscopy (STM) performed by Liang et al. has also indicated a band

gap of ~2.0 eV for phsophorene.[19,20] Therefore, GW method is very credible in accurately describing the band structure of phosphorene. However, the wide applications of GW are significantly restricted by the huge computing-resource consumption.

As a compromise, hybrid DFT which can relieve the band gap underestimation of pure DFT and consume less computing time than the GW method, is attractive in exploring the band structure of materials. Currently, the Heyd–Scuseria–Ernzerhof (HSE) hybrid functional which is based on the PBEh hybrid functional turns out to be preferable in determining the band gap of semiconductors. The HSE exchange-correlation energy is based on an expression below:[21]

$$E_{XC}^{HSE} = aE_x^{HF,SR}(\omega) + (1-a)E_x^{\omega PBE,SR}(\omega) + E_x^{\omega PBE,LR}(\omega) + E_c^{PBE}$$

where $E_x^{HF,SR}$ is the short-range Hartree Fock (HF) exchange. $E_x^{\omega PBE,SR}$ and $E_x^{\omega PBE,LR}$ are the short- and long-range components of the PBE exchange functional, ω is the splitting parameter and a (=1/4) is the HF mixing constant. By setting the value of ω appropriately, one can obtain a reasonable band gap. Commonly, ω is set to be 0.2, corresponding to the HSE06 functional. With HSE06, the band gap of phosphorene is computed to be ~1.5 eV,[11,22] still lower than the GW predicted and the experimental measured values.

For the band gap computation of phosphorene, another attractive method is the modified Becke and Johnson (mBJ) method which gives a close band gap (~1.4 eV) to that predicted by HSE06, as shown in Table 1. The mBJ method is developed by minimizing the mean absolute relative error for the band gap of abundant solids and is as cheap as LDA or GGA. Thus, the mBJ method is advantageous to be applied in large systems.[23] However, as the mBJ method is based on experimental fitting, it shows different accuracies to different materials. Moreover, in the mBJ method, only the exchange-correlation potential is proposed, while the exchange-correlation functional is defected. Therefore, mBJ would confront difficulties in self-consistent convergence for some systems.

Although pure DFT methods (such as PBE and mBJ) and hybrid DFT (such as HSE06) underestimate the band gap of phosphorene at different levels, they actually deliver identical physical picture with GW method. For example, both PBE and HSE06 computations demonstrate that phosphorene is semiconducting with a quasi-direct band gap, with the conduction band minimum (CBM) located at the Γ point and the valence band maximum (VBM) situated close to the Γ point,[11,24] consistent with the GW computation. As the energy difference between the Γ point and the actual VBM is lower than 10 meV, phosphorene can still be considered as a direct band-gap semiconductor. The computed band gap of phosphorene via various methods is summarized in Table 1 in comparison with experimental results.

As seen from the band structure of phosphorene (Figure 1(b)), conduction and valence bands in the y direction (Γ-Y) are more flat than those in the x direction (Γ-X), indicating a highly asymmetric band structure for phosphorene, and thus contributes to anisotropic excitons and effective mass in different orientations.[25,26] As revealed by HSE06 computations, the effective mass in the x direction is 0.15 m_0 for holes and 0.17 m_0 for electrons, while in the y direction the effective mass is 6.35 m_0 for holes and 1.12 m_0 for electrons.[11] The anisotropic effective mass in the x and y directions for electrons and holes indicates that phosphorene could possess anisotropic carrier mobility in the x and y directions, which is another important factor besides the band gap for semiconductors in device applications.

Computationally, the carrier mobility of semiconductors can be evaluated by deformation potential (DP) theory which was initially proposed by Barden and Shockley.[27] According to the DP theory, the respective energies of the CBM and VBM have a linear relationship with the lattice dilation or compression. The carrier mobility (μ) of 2D materials can be given by the following expression:[11]

$$\mu = \frac{2e\hbar^3 C}{3k_B T|m^*|^2 E_1^{\,2}}$$

where $\hbar$ is reduced Planck constant, k_B is Boltzmann constant, and T is the temperature, while m^*, E_1, and C are the effective mass, DP constant, and in-plane stiffness of the studied 2D material, respectively.

At the HSE06 level of theory, Qiao et al. indicated that the electron mobility along the x direction in phosphorene is about 1100–1140 cm^2/Vs, almost 14 times higher than that in the y direction (~80 cm^2/Vs).[11] However, the hole mobility in the x direction (640–700 cm^2/Vs) of phosphorene is 16–38 times lower than that in the y direction (10,000–26,000 cm^2/Vs), which indicates the high-mobility transport anisotropy in phosphorene. Remarkably, the extraordinary carrier mobility of phosphorene is much higher than that of MoS_2 (~200 cm^2/Vs).[28] As a consequence, the high-carrier mobility and moderate direct band gap of

phosphorene render it a promising candidate for fabricating transistors. Moreover, the electron/hole mobility anisotropy along the x and y directions also promises phosphorene valuable potentials for electron and hole separations.

Note that the band structure of phosphorene is significantly sensitive to the number of layers. Both computational and experimental investigations have demonstrated that phosphorene possesses a layer-dependent direct band gap.[19,29] Especially, with increasing the layer thickness, the band gap of phosphorene decreases monotonically.[11,19,30] Rudenko et al. suggested that the thickness-dependent band structure of phosphorene can be ascribed to the repulsive interlayer hopping effect.[31] Besides thickness, Dai et al. revealed theoretically that the electronic properties of phosphorene layers also have a close relationship with stacking patterns.[29] Therefore, the electronic properties of phosphorene can be effectively tuned by controlling the thickness and stacking patterns.

Optical and Thermal Properties

The absorption spectrum of phosphorene can be predicted by computing the dielectric function, which is defined as $\varepsilon(\omega) = \varepsilon_1(\omega) + i\varepsilon_2(\omega)$. The imaginary part $\varepsilon_2(\omega)$ of dielectric function can be expressed by[32]:

$$\varepsilon^2_{\alpha\beta}(\omega) = \frac{4\pi^2 e^2}{\Omega} \lim_{q\to 0} \frac{1}{q^2} \sum_{c,v,\vec{k}} 2w_{\vec{k}}\, \delta\left(\varepsilon_{c\vec{k}} - \varepsilon_{v\vec{k}} - \omega\right) \times \left\langle u_{c\vec{k}+e_\alpha \vec{q}} \middle| u_{v\vec{k}} \right\rangle \left\langle u_{c\vec{k}+e_\beta \vec{q}} \middle| u_{v\vec{k}} \right\rangle^*$$

where the indices c and v refer to the conduction and valence band states, respectively, and $u_{c\vec{k}}$ is the cell periodic part of the orbitals at the k-point $\vec{k}$. The real part $\varepsilon_1(\omega)$ could be obtained from the imaginary part $\varepsilon_2(\omega)$ of dielectric function by Kramer–Kronig relationship. Based on the calculated dielectric function, Qiao et al. revealed that phosphorene shows optical anisotropy along the x and y directions, resulting in a strong linear dichroism.[11] Specifically, phosphorene has absorption at 1.55 eV with incident light in the x direction, while light absorption happens at 3.14 eV in the y direction. Owing to the strong linear dichroism, the orientation of phosphorene can be experimentally determined by using optical spectroscopy.

DFT computations by Cai et al. indicated that phosphorene monolayer can allow faster phonons transport along the y direction than that along the x direction.[33] This anisotropic phonon property leads to an asymmetrical thermal conductivity for phosphorene. Using the nonequilibrium Green's function (NEGF) method combined with first-principles computations, Ong et al. predicted that phosphorene monolayer has a significant thermal transport anisotropy.[34] At room temperature, the thermal conductance along the y direction of phosphorene can be 40% higher than that along the x direction. Similarly, via DFT and density functional perturbation theory (DFPT) computations, Jain et al. predicted that phosphorene monolayer can be qualified with a thermal conductivity of 36 and 110 W/mK along the x and y directions at 300 K, respectively.[35] The comparable thermal conductivity to that of MoS_2 makes phosphorene attractive for thermal transport.[36] Moreover, Fei et al. predicted that phosphorene also possesses an anisotropic electrical conductance which is orientation orthogonal to the anisotropic thermal conductance, thus resulting in a high ratio of electrical conductance against thermal conductance for phosphorene.[37] As a consequence, phosphorene can convert heat energy to electrical energy with high efficiency, which is desirable for thermoelectrics.

Inspiringly, some of the theoretically predicted electronic and optical properties of phosphorene besides its carrier mobility have been well verified by experimental investigations. For example, Zhang et al. revealed that few-layer phosphorene shows strong and layer-dependent photoluminescence (PL) and anisotropic Raman response.[38] As shown in Figure 2(a) and (b), the PL peaks show blue shift with increasing layer thickness, indicating consistent results with those of computations, and experimentally verifying the thickness-dependent band gap of phosphorene. They also demonstrated that the Raman phonon modes, A_g^1, B_{2g}, and A_g^2, of phosphorene show blue shift with decreasing temperature. The sensitive response of phonon frequency to temperature modulation should be ascribed to the mechanical flexibility of phosphorene. Moreover, by performing linearly polarized Raman measurements, it was demonstrated that the anisotropic Raman response can be utilized to quickly determine the crystalline orientation of phosphorene,[39] echoing well with the theoretical prediction.[11]

PROPERTY TUNING

To widen the applications of phosphorene in more fields, various methods have been theoretically proposed to tune the properties of phosphorene, including external elastic strain,[24,40,41] external electric field,[42] surface modification with atomic defects,[43]

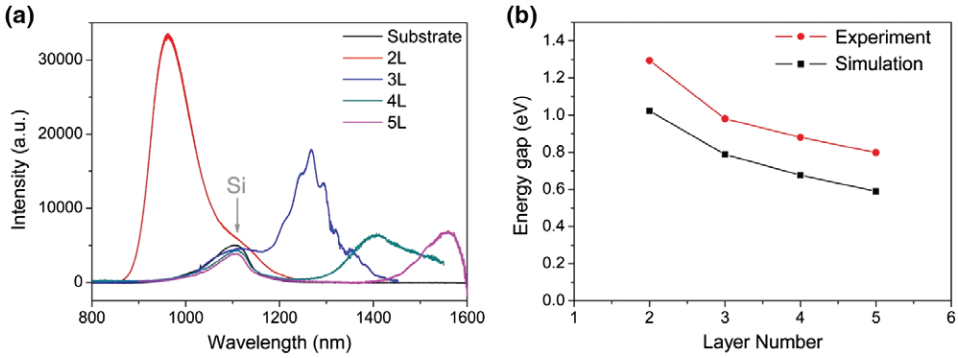

FIGURE 2 | (a) Photoluminescence (PL) spectra of few layer phosphorene and (b) band gap of few-layer phosphorene from PL measurements and computations. (Reproduced with permissions from Ref 38 Copyright 2014 American Chemical Society)

molecule doping,[44] and size regulation in tailored nanoribbons.[45]

External Elastic Strain

Owing to the mechanical flexibility and anisotropy of phosphorene, elastic strain works dramatically in tuning the properties of phosphorene. As demonstrated by various computations, elastic strain can cause a direct–indirect band gap transition as well as semiconducting-metallic transition for phosphorene. As shown in Figure 3(a), DFT–PBE computations demonstrated that the band gap of phosphorene increases to a maximum with certain (4%) tensile strain in the *y* (zigzag) direction and then decreases with increasing the strain.[40] When subjected to a compressive strain in the *y* direction, the band gap decreases with increasing the strain, and can be closed finally. Similar strain-tuning results were also found in the *x* direction, as shown in Figure 3(b). GGA–PBE and HSE06 computations both predicted that under a biaxial strain, the band structure of phosphorene varies more prominently and requires an even lower critical strain to trigger the semiconducting-metallic and direct–indirect transitions.[41] Although DFT underestimates the band gap of phosphorene, the predicted trend for strain modulations is solid.

However, for the prediction of semiconductor–metal transition point, GW is more reliable. Via GW computations, Çakır et al. revealed that elastic strain also has significant effects on the optical properties of phosphorene.[41] As shown in Figure 3(c), the optical gap of phosphorene increases with increasing the biaxial tensile strain at first. Under a biaxial tensile strain of 4%, phosphorene can be active over the most visible range. The further increase of tensile strain, however, would decrease the optical gap. When subjected to a biaxial compressive strain, the optical gap monotonically decreases as the increase of strain. By means of DFT (LDA) computations, Fei et al. studied the lattice vibrational mode and corresponding Raman spectra of phosphorene under both uniaxial and biaxial strains along two directions.[46] According to their results, applying axial strains can effectively modulate the frequency and intensity of three typical Raman scattering signals, namely A_g^1, B_{2g}, and A_g^2 modes, as shown in Figure 3(d). Especially, the energy spacing between A_g^1 and B_{2g} modes increases under tensile strain and decreases under compressive strain in the armchair (*x*) direction (Figure 3(e)), while alters oppositely in the zigzag (*y*) direction (Figure 3(f)).

Fei et al. further demonstrated that the carrier mobility of phosphorene can be controlled by applying elastic strain via DFT-PBE computations.[47] Under a 5% biaxial strain, the electric effective mass of phosphorene can be rotated by exactly 90°, thus contributes to more effective electron mobility in the *y* direction opposite to the case in strain-less phosphorene. Moreover, the effect of compressive strain on the carrier mobility is more pronounced for bilayer phosphorene.[48] Computed at the HSE06 level of theory, Morgan et al. indicated that a perpendicular compressive strain can enhance the electron mobility of bilayer phosphorene by two orders of magnitude. Especially, the thermal conductivity of phosphorene can also be modulated by elastic strain. For example, by means of DFT/PBE combined with the semi-classical Boltzmann transport theory, Lu et al. revealed that the Seebeck coefficient can be greatly enhanced under the tensile strain applied in both zigzag and armchair directions.[49]

Electric Field

Experimental investigations have also proved that the gate voltage can effectively modulate the drain

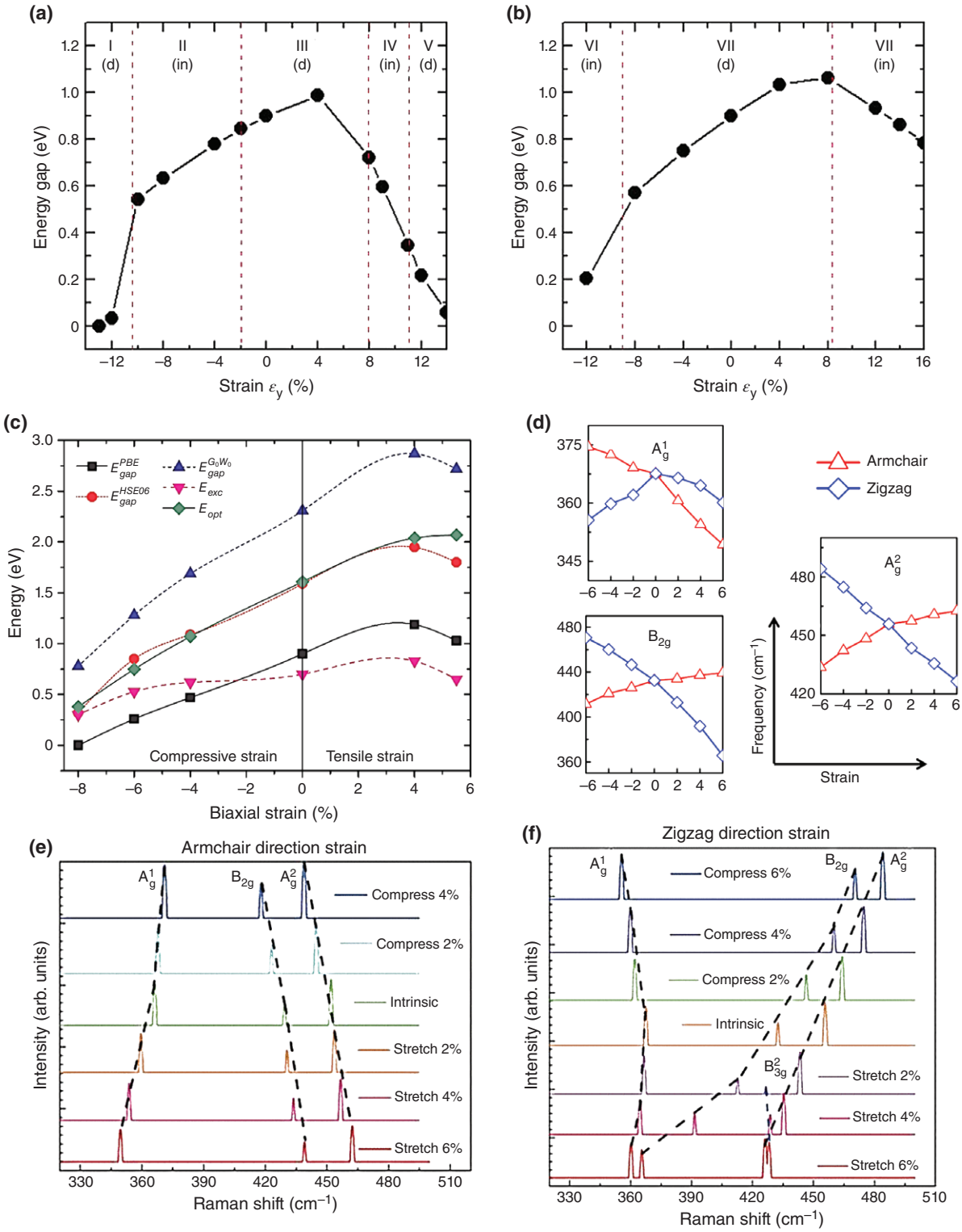

FIGURE 3 | The band gap of phosphorene as a function of the applied uniaxial strain along zigzag (a) and armchair (b) directions. Zones I, II, III, IV, V, VI, VII, and VIII are divided by the direct (d) or indirect (in) band gap of phopshorene under corresponding uniaxial strain.(c) Electronic band gap ($E_{\text{gap}}^{\text{PBE}}$, $E_{\text{gap}}^{\text{HSE06}}$ and $E_{\text{gap}}^{\text{G}_0\text{W}_0}$), optical gap ($E_{\text{opt}}$), and exciton-binding energy (E_{exc}) of phosphorene as a function of biaxial strain for different exchange-correlation functionals. (d) Frequencies of modes A_g^1, B_{2g}, and A_g^2, for phosphorene under uniaxial strain. Raman spectra of phosphorene under uniaxial strain along armchair (e) and zigzag (f) directions. (Reproduced with permissions from Ref 40 Copyright 2014 American Physical Society; Ref 41 Copyright 2014 American Physical Society; Ref 46 Copyright 2014 AIP Publishing LLC)

current and conductance of few-layer phosphorene transistors.[5] Very recently, via DFT/PBE computations, Liu et al. have revealed that under a vertical electric field, few-layer (1–4 layer) phosphorene can be transformed from a normal insulator to an intriguing topological insulator.[42] Specifically, this transition happens under the critical electric field of 0.55 and 0.3 V/Å for 3- and 4-layer phosphorene, respectively. The band structures of 4-layer phosphorene under different external electric fields are shown in Figure 4(a)–(d). As shown in Figure 4(d), 4-layer phosphorene becomes metallic when the electric field is 0.6 V/Å. Aware of that PBE could seriously underestimate the band gap, Liu et al. also examined the effect of electric field on electronic properties of phosphorene layer by using HSE06 hybrid functional and found the same trend as that predicted by PBE functional but with a higher critical electric field. Inspiringly, Kim et al. have experimentally demonstrated that the band gap of few-layer phosphorene can be effectively tuned by a vertical electric field through band structure measurements.[50,51] At a critical electric field, the semiconducting few-layer phosphorene can be tuned to be a Dirac semimetal, which confirms the theoretical predictions.[42] Therefore, applying electric field is an important and dependable method to tune the properties of phosphorene.

Surface Modifications

Surface modification is also an effective approach toward engineering the properties of phosphorene. Vacancy and topological defects on phosphorene are inevitable during the preparation process and can affect the properties of phosphorene.[52] Srivastava et al. demonstrated theoretically that a monovacancy defect in phosphorene can induce magnetization while phosphorene with a divacancy defect is nonmagnetic.[43] Adsorption of N, Fe, Co, Cr, or Au adatoms can also make phosphorene magnetic.[43,53] However, the magnetic states for those transition metal (TM) atom doped phosphorene are quite different.[54] For example, codoped phosphorene is nonmagnetic while those Ti-, V-, Cr-, Mn-, Fe-, or Ni-doped phosphorene are magnetic. Substitution P atom with nonmetallic elements, such as Si, S, and Cl, can also introduce local magnetic moments for phosphorene.[55]

Aside from atomic modification, molecular adsorption also turns out to be effective in tuning the electronic properties of phosphorene. Cai et al. reported that small molecules, such as CO, H_2, H_2O, NH_3, NO, NO_2, and O_2 can be physisorbed on the surface of phosphorene with significant charge transfer from molecules (CO, H_2, H_2O, and NH_3) to phosphorene or from phosphorene to molecules (O_2 and NO_2).[44] These molecular physisorption can effectively modulate the charge carrier density of phosphorene and also render it promising for gas sensors. DFT/PBE computations indicated that charge transfer can also happen between phosphorene and organic molecules, including tetracyanoquinodimethane (TCNQ), tetracyanoethylene (TCNE), and tetrathiafulvalene (TTF).[56,57] Especially, the adsorption of these molecules can induce in-gap states in the band structure of phosphorene, leading to significant band gap reduction for phosphorene.

Phosphorene Nanoribbons

Cutting 2D materials into quasi 1D nanoribbons can bring many novel properties due to the quantum confinement effect and the probable edge states. The electronic properties of phosphorene nanoribbons (PNRs) have been extensively investigated theoretically. As shown in Figure 5(a)–(d), zigzag PNRs

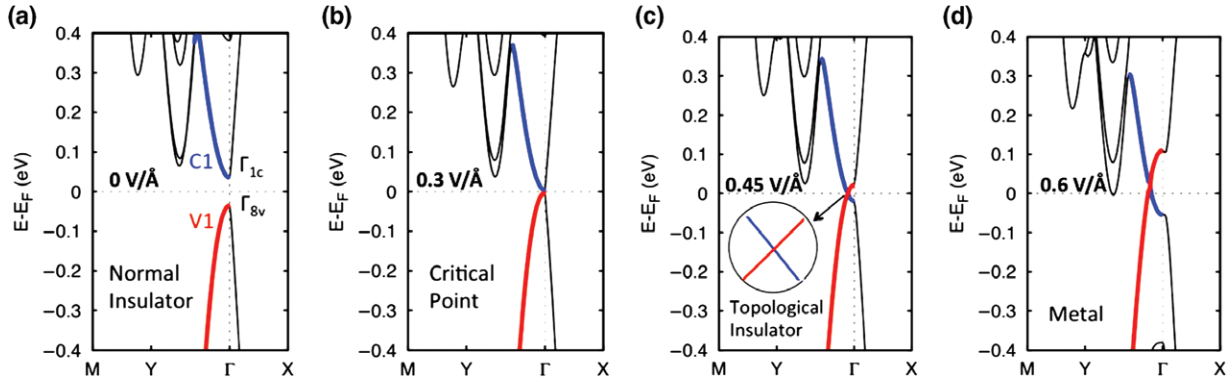

FIGURE 4 | Band structure of 4-layer phosphorene under external electric field of (a) 0 V/Å, (b) 0.3 V/Å, (c) 0.45 V/Å, and (d) 0.6 V/Å at PBE level. (Reproduced with permissions from Ref 42 Copyright 2015 American Chemical Society)

(zPNRs), armchair PNRs (aPNRs), and diagonal PNRs (dPNRs) can be obtained by cutting 2D phosphorene along three different directions. Guo et al. revealed that bare aPNRs are all semiconducting with an indirect band gap, which decreases with increasing the ribbon width. In contrast, all bare zPNRs are metallic regardless of the ribbon width.[45] Zhu et al. further demonstrated that the dangling band states in bare zPNRs are ferromagnetically coupled in one edge but antiferromagnetically coupled between two edges.[58] However, both aPNRs and zPNRs become semiconducting with a direct band gap after hydrogen termination.[59]

As shown in Figure 5(e), Han et al. indicated that the band gap of hydrogen terminated PNRs decreases with increasing the ribbon width.[60] They also found that the carrier effective mass of hydrogen terminated aPNRs (H-aPNRs) are smaller than those of zigzag and diagonal ones. Especially, the band gap and carrier effective mass of H-aPNRs can be effectively modulated by applying elastic strain (Figure 5(f)), and thus facilitate the wide applications of H-aPNRs. Moreover, consistent with the optical anisotropy of phosphorene, hydrogen terminated zPNRs (H-zPNRs) show higher absorption edge energies than those of H-aPNRs with similar width.[61]

POTENTIAL APPLICATIONS

With such fantastic geometric, mechanical, electronic, optical, and thermal properties, phosphorene shows potential applications in many important fields. The first application of phosphorene is in transistors following its experimental exfoliation. However, experimentally detected carrier mobility of phosphorene is lower than the theoretically predicted value because the prepared phosphorene may possess uncontrollable surface and edge defects and also has inhomogenous thickness. Nevertheless, the experimentally examined carrier mobility of phosphorene (~1000 $cm^2V^{-1}second^{-1}$),[5,62] is much larger than that of MoS_2 and comparable to that of graphene devices,[63] and thus renders phsophorene an attractive 2D transistor material.

The appropriate band gap of phosphorene also makes it attractive for light harvesting and photocatalysis. Using DFT computations, Sa et al. predicted that phosphorene can be an effective photocatalyst for water splitting at a given pH of 8.[22] They also revealed that the water splitting process on phosphorene is energetically favorable and can be improved by applying a strain.

Theoretical studies have also been performed to explore the possible applications of phosphorene in

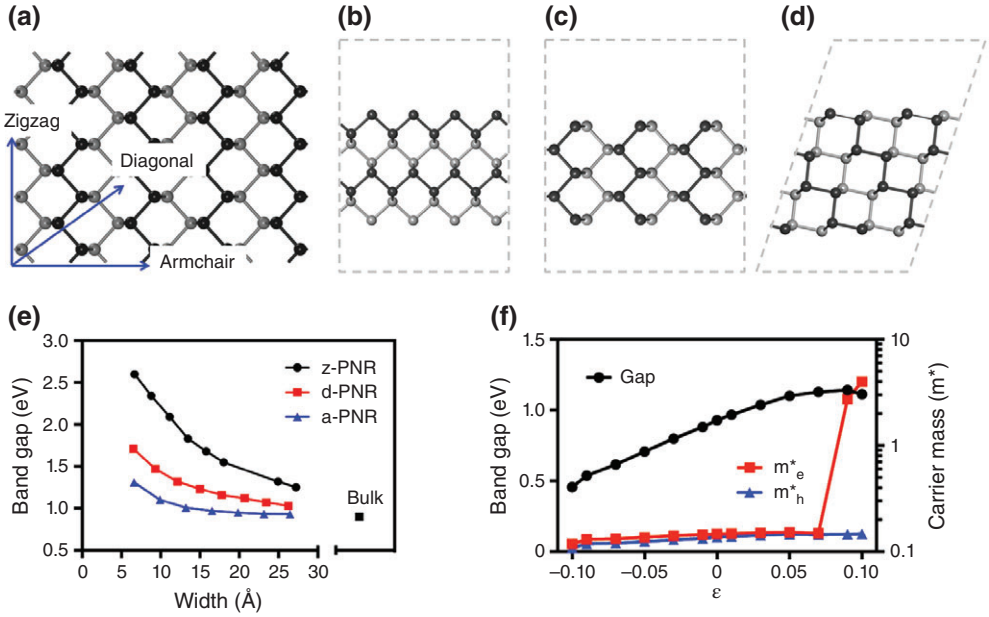

FIGURE 5 | (a) Schematic of two-dimensional (2D) phosphorene with armchair, zigzag, and diagonal directions labeled. Structure of zigzag phosphorene nanoribbon (b), armchair phosphorene nanoribbon (c), and diagonal phosphorene nanoribbon (d); (e) Variation of band gap with increasing the ribbon width for zPNR, aPNR, and dPNR with hydrogen termination, respectively; (f) Band gap and effective electron mass (m^*_e) and hole mass (m^*_h) of H-aPNRs as functions of elastic strain. (Reproduced with permissions from Ref 60 Copyright 2014 American Chemical Society)

lithium-ion batteries (LIBs) and sodium-ion batteries (SIBs). Via DFT/PBE computations, Zhao et al. revealed that phosphorene can be a good anode material in LIBs.[64] The theoretical capacity of phosphorene monolayer is predicted to be as high as 433 mA h g^{-1}, making phosphorene attractive for high capacity LIBs. DFT computations further demonstrated that phosphorene shows anisotropy for Li diffusion. Compared with the high diffusion barrier of 0.68 eV along armchair direction in phosphorene monolayer (Figure 6(a) and (b)), Li et al. reported that the diffusion of Li is highly favored along the zigzag direction (Figure 6(c) and (d)) with a negligible diffusion barrier of 0.08 eV.[65] As a comparison, the diffusion barriers of Li on graphene (~0.33 eV) and MoS_2 monolayer (~0.25 eV) are much higher than that on phosphorene along the zigzag direction.[66,67] Thus, the highly favored Li diffusion of phosphorene would render it an attractive anode material with marvelous high-rate performance. Diffusion barrier profiles for Li along armchair and zigzag directions on phosphorene are shown in Figure 6(e). Via DFT/PBE computations, Kulish et al. further predicted the potentials of phosphorene for Na storage, including high-theoretical capacity (433 mA h g^{-1}), low diffusion barrier (0.04 eV) and good electrical conductivity.[68] Very recently, Sun et al. have prepared a hybrid material made out of few phosphorene layers sandwiched between graphene layers, and applied it as anode material for SIBs.[69] As revealed by this experimental study, phosphorene-based anodes show high capacity and good stability for SIBs. Therefore, based on those theoretical and experimental investigations, phosphorene will be a promising material for energy storage.

NEW PHASE EXPLORATIONS

Extensive theoretical studies have revealed that phosphorene monolayer can also crystallize in other phases in addition to the most stable black phosphorus phase. The structural and electronic properties of many metastable phosphorene monolayers have been theoretically investigated. The most attractive allotrope of metastable phosphorene monolayer is blue phosphorene, denoted as β-P, which is quite close in energy to black phosphorene monolayer (denoted as α-P for comparison).[70] With a hexagonal lattice, β-P is actually the structural analogue of silicene and germanene and exhibits isotropic structure (Figure 7(a)). As shown in Figure 7(d), β-P is also semiconducting with an indirect band gap of ~2 eV.[70] Interestingly, the band gap of β-P increases with increasing the thickness, which is in contrast to that of α-P. At present, β-P is still a hypothetical material which has not been realized experimentally. Zhu et al. predicted that β-P can be synthesized by using practical substrates in chemical vapor deposition growth. Via the combination of molecular dynamics (MD) and Monte Carlo (MC) simulations, Boulfelfel et al. predicted that blue phosphorus may be realized by pressure-induced phase transition in black phosphorus.[71] Then, it will be feasible to exfoliate blue phosphorus into monolayers because the interlayer interaction in blue phosphorus is weaker than that in black phosphorus.

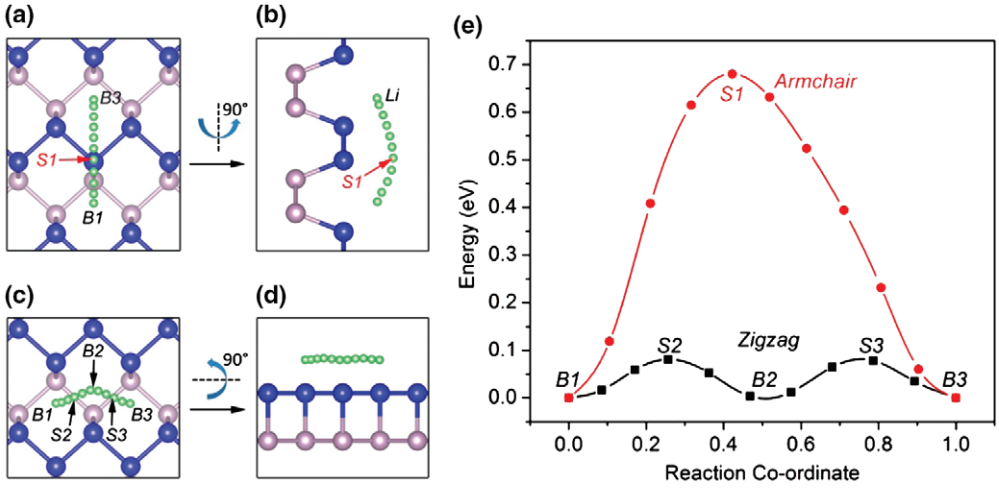

FIGURE 6 | Diffusion path of Li on phosphorene along the armchair (a and b) and zigzag directions (c and d) from the top and side view; Energy profiles for Li diffusion on phosphorene along armchair and zigzag directions (e). (Reproduced with permissions from Ref 65 Copyright 2015 American Chemical Society)

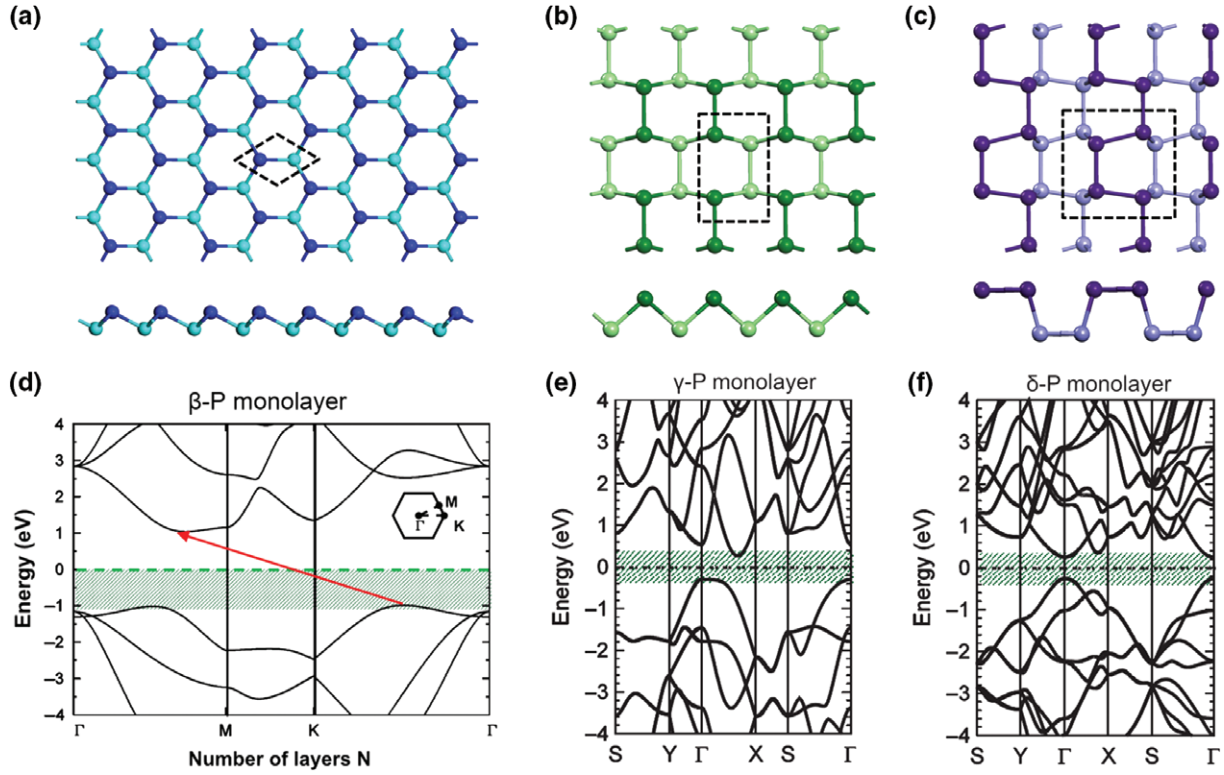

FIGURE 7 | Schematics of β-P (a), γ-P (b), and δ-P (c) monolayer in top and side views. In each schematic, the P atoms in top layer are assigned by dark atoms and light atoms denote P in bottom layer. Band structure of β-P (d), γ-P (e), and δ-P (f) monolayer. (Reproduced with permissions from Ref 70 Copyright 2014 American Physical Society; Ref 72 Copyright 2014 American Physical Society)

TABLE 2 | Lattice Constants *a* and *b*, Energy Difference ($\Delta E_{eV/atom}$) Relative to α-P and Band Gap (Value and Type) for Phosphorene in Different Phases, Predicted by DFT Computations

	α-P	β-P	γ-P	δ-P	ε-P	ζ-P	η-P	θ-P
a/Å	4.58	3.33	3.41	5.56	5.37	6.43	5.40	5.50
b/Å	3.32	3.33	5.34	5.46	5.37	5.32	6.32	6.22
$\Delta E_{eV/atom}$	0	0.02	0.10	0.08	0.13	0.10	0.05	0.01
E_{gap}/eV	1.51	2.0	0.50	0.45	0.25	1.19	0.87	1.16
Bandgap	Direct	Indirect	Indirect	Direct	Direct	Indirect	Indirect	Indirect
Refs	11	70	72	72	73	73	73	73

DFT, density functional theory.

After α-P and β-P, γ-phase and δ-phase allotropes of phosphorene were proposed by Guan et al.[72] As shown in Figure 7(b) and (c), both γ- and δ-P have a rectangular unit cell, which contains 4 and 8 P atoms, respectively. The computed lattice parameters for γ-P and δ-P can be found in Table 2. Computed at the PBE level of theory, γ-P is semiconducting with an indirect band gap of 0.5 eV (Figure 7 (e)), while δ-P has a direct band gap of 0.45 eV (Figure 7(f)).

Very recently, Wu et al. have further enriched the phases of phosphorene by proposing several new polytypes composed of P4 square or P5 pentagon units, including ε-P, ζ-P, η-P, and θ-P.[73] The similar cohesive energy for different phosphorene configurations indicates the comparable stability of different phosphorene allotropes, as shown in Table 2. By performing Born–Oppenheimer molecular dynamics (BOMD) and phonon dispersion simulations, the good thermal and dynamic stability of ε-P, ζ-P, η-P, and θ-P was further confirmed. These four phosphorene polytypes are all semiconducting (Table 2). Specifically, the band gap of ε-P is direct while those of ζ-P, η-P, and θ-P are indirect.

Currently, phosphorene phases except α-P are still discussed at the theoretical level. However, as implied by DFT computations, these new phases of phosphorene show comparable formation feasibility and stability to α-P, which are highly promising to be experimentally realized. Therefore, theoretical investigations have significantly helped understand possible phosphorene phases and promoted the development of phosphorene in a wide scale.

PROSPECTIVE AND CONCLUSION

Although extensive studies have been performed to promote the investigations of phosphorene, there are still problems restricting its development. As revealed by an experimental study, significant surface roughening of thin phosphorene was observed via atomic force microscopy (AFM) after exfoliation,[74] implying the instability of phosphorene. Lu et al. has recently demonstrated that laser pruning approach can be used to prepare few-layer phosphorene under ambient conditions.[75] However, the laser induces different degrees of oxidation to phosphorene as well. DFT computations also indicated that phosphorene can be easily etched by O_2 at ambient atmosphere.[76] Therefore, for the wide applications of phosphorene, the instability issue should be conquered in future studies. Enlightened by the fact that composites with graphene can well stabilize few-layer structures (such as MoS_2) from restacking, it has been suggested that phosphorene would be stabilized by interacting with graphene or other 2D materials.[77] Inspiringly, phosphorene-MoS_2 heterojunction p-n diodes have been fabricated through vdW interactions between phosphorene and MoS_2.[78] Meanwhile, DFT computations also indicated that phosphorene/graphene and phosphorene/BN heterostructures could be stabilized via weak interlayer noncovalent bonding, which indicates a possible way to protect phosphorene from structural and chemical degradation.[79] Very recently, Avsar et al. have experimentally realized the encapsulation of thin layer black phosphorus and graphene with hexagonal BN in a layer-by-layer fashion.[80] As a result, electric field transistors with the encapsulated thin layer black phosphorus show excellent stability over 2 weeks and present hysteresis-free transport characteristics, which verifies the DFT computational predictions. Therefore, the technique of creating 2D heterostructures can be effectively utilized to control or suppress the oxidation of phosphorene.

As large-scale phosphorene is still experimentally inaccessible, effective and facile methods to prepare phosphorene should be developed to facilitate its wide applications. Very recently, Sresht et al. have theoretically investigated the liquid-phase exfoliation process of phosphorene in different solvents via modeling the solvent-phosphorene interactions using MD simulations.[81] They indicated that if the solvent has planarity and the cohesion between the solvent molecules and the adhesion between phosphorene and molecules are equivalently strong, the exfoliation and dispersion of phosphorene nanosheets in the solvent will be favorable. Therefore, finding suitable solvents may help realize the preparation of large-scale phosphorene via liquid exfoliation in the near future.

In this overview, the fast development of phosphorene in the past year is briefly summarized, particularly from the view of computational side. By introducing the intrinsic properties, possible applications, and new phosphorene phases, we can know much about phosphorene from computations. On the basis of first-principles computations, phosphorene is predicted to have anisotropic mechanical, electronic, magnetic, optical, and thermal properties due to its anisotropic configuration. Those fantastic properties of phosphorene can be further tuned by elastic strain, external electric field, atomic and molecular doping, and thickness and width control. Inspiringly, the direct band-gap semiconducting property, high-charge carrier mobility, and wide-range light absorption of phosphorene have been verified experimentally, which make phosphorene a promising 2D material with wide applications. The theoretical explorations to the new phases of phosphorene have promoted the understanding of P in 2D configurations and provide reliable guidance for experiments. We hope that our overview on phosphorene from the computational side can help better understand the present investigations of phosphorene and shed lights on the development of phosphorene and other novel 2D materials for wider applications.

ACKNOWLEDGMENTS

This work was supported by NSFC (21273118 and 21421001) and MOE Innovation Team (IRT13022) in China.

FURTHER READING

Akai T, Endo S, Akahama Y, Koto K, Marljyama Y. The crystal structure and oriented transformation of black phosphorus under high pressure. *High Press Res* 1989, 1:115–130.

Yoshizawa M, Shirotani I, Fujimura T. Thermal and elastic properties of black phosphorus. *J Physical Soc Japan* 1986, 55:1196–1202.

Zhang J, Liu HJ, Cheng L, Wei J, Liang JH, Fan DD, Shi J, Tang XF, Zhang QJ. Phosphorene nanoribbon as a promising candidate for thermoelectric applications. *Sci Rep* 2014, 4:6452.

Sorkin V, Zhang YW. The structure and elastic properties of phosphorene edges. *Nanotechnology* 2015, 26:235707.

Sorkin V, Zhang YW. The deformation and failure behaviour of phosphorene nanoribbons under uniaxial tensile strain. *2D Mater* 2015, 2:035007.

REFERENCES

1. Liu H, Du Y, Deng Y, Ye PD. Semiconducting black phosphorus: synthesis, transport properties and electronic applications. *Chem Soc Rev* 2015, 44:2732–2743.
2. Brown A, Rundqvist S. Refinement of the crystal structure of black phosphorus. *Acta Crystallogr* 1965, 19:684–685.
3. Churchill HOH, Jarillo-Herrero P. Two-dimensional crystals: phosphorus joins the family. *Nat Nanotechnol* 2014, 9:330–331.
4. Reich ES. Phosphorene excites materials scientists. *Nature* 2014, 506:19.
5. Li L, YuY YGJ, Ge Q, Ou X, Wu H, Feng D, Chen XH, Zhang Y. Black phosphorus field-effect transistors. *Nat Nanotechnol* 2014, 9:372–377.
6. Liu H, Neal AT, Zhu Z, Luo Z, Xu X, Tománek D, Ye PD. Phosphorene: an unexplored 2D semiconductor with a high hole mobility. *ACS Nano* 2014, 8:4033–4041.
7. Brent JR, Savjani N, Lewis EA, Haigh SJ, Lewis DJ, O'Brien P. Production of few-layer phosphorene by liquid exfoliation of black phosphorus. *Chem Commun* 2014, 50:13338–13341.
8. Lu W, Nan H, Hong J, Chen Y, Zhu C, Liang Z, Ma X, Ni Z, Jin C, Zhang Z. Plasma-assisted fabrication of monolayer phosphorene and its Raman characterization. *Nano Res* 2014, 7:853–859.
9. Takao Y, Morita A. Electronic structure of black phosphorus: tight binding approach. *Physica B + C* 1981, 105:93–98.
10. Asahina H, Morita A. Band structure and optical properties of black phosphorus. *J Phys C: Solid State Phys* 1984, 17:1839–1852.
11. Qiao J, Kong X, Hu ZX, Yang F, Ji W. High-mobility transport anisotropy and linear dichroism in few-layer black phosphorus. *Nat Commun* 2014, 5:4475.
12. Grimme S. Density functional theory with London dispersion corrections. *WIREs Comput Mol Sci* 2011, 1:211–228.
13. Klimeš J, Bowler DR, Michaelides A. Van der Waals density functionals applied to solids. *Phys Rev B* 2011, 83:195131.
14. Jiang JW, Park HS. Mechanical properties of single-layer black phosphorus. *J Phys D Appl Phys* 2014, 47:385304.
15. Wei Q, Peng X. Superior mechanical flexibility of phosphorene and few-layer black phosphorus. *Appl Phys Lett* 2014, 104:251915.
16. Jiang JW, Park HS. Negative poisson's ratio in single-layer blackphosphorus. *Nat Commun* 2014, 5:4727.
17. Appalakondaiah S, Vaitheeswaran G, Lebègue S, Christensen NE, Svane A. Effect of van der Waals interactions on the structural and elastic properties of black phosphorus. *Phys Rev B* 2012, 86:035105.
18. Hybertsen MS, Louie SG. Electron correlation in semiconductors and insulators: Band gaps and quasiparticle energies. *Phys Rev B* 1986, 34:5390.
19. Tran V, Soklaski R, Liang Y, Yang L. Layer-controlled band gap and anisotropic excitons in few-layer black phosphorus. *Phys Rev B* 2014, 89:235319.
20. Liang L, Wang J, Lin W, Sumpter BG, Meunier V, Pan M. Electronic bandgap and edge reconstruction in phosphorene materials. *Nano Lett* 2014, 14:6400–6406.
21. Heyd J, Peralta JE, Scuseria GE. Energy band gaps and lattice parameters evaluated with the Heyd-Scuseria-Ernzerh of screened hybrid functional. *J Chem Phys* 2005, 123:174101.
22. Sa B, Li YL, Qi J, Ahuja R, Sun Z. Strain engineering for phosphorene: the potential application as a photocatalyst. *J Phys Chem C* 2014, 118:26560–26568.
23. Tran F, Blaha P. Accurate band gaps of semiconductors and insulators with a semilocal exchange-

correlation potential. *Phys Rev Lett* 2009, 102:226401.

24. Rodin AS, Carvalho A, Castro Neto AH. Strain-induced gap modification in black phosphorus. *Phys Rev Lett* 2014, 112:176801.
25. Low T, Roldán R, Wang H, Xia F, Avouris P, Moreno LM, Guinea F. Plasmons and screening in monolayer and multilayer black phosphorus. *Phys Rev Lett* 2014, 113:106802.
26. Rodin AS, Carvalho A, Castro Neto AH. Excitons in anisotropic two-dimensional semiconducting crystals. *Phys Rev B* 2014, 90:075429.
27. Bardeen J, Shockley W. Deformation potentials and mobilities in non-polarcrystals. *Phys Rev* 1950, 80:72–80.
28. Cai Y, Zhang G, Zhang YW. Polarity-reversed robust carrier mobility in monolayer MoS_2 nanoribbons. *J Am Chem Soc* 2014, 136:6269–6275.
29. Dai J, Zeng XC. Bilayer phosphorene: effect of stacking order on bandgap and its potential applications in thin-film solar cells. *J Phys Chem Lett* 2014, 5:1289–1293.
30. Das S, Zhang W, Demarteau M, Hoffmann A, Dubey M, Roelofs A. Tunable transport gap in phosphorene. *Nano Lett* 2014, 14:5733–5739.
31. Rudenko AN, Katsnelson MI. Quasiparticle band structure and tight-binding model for single- and bilayer black phosphorus. *Phys Rev B* 2014, 89:201408.
32. Gajdoš M, Hummer K, Kresse G. Linear optical properties in the projector-augmented wave methodology. *Phys Rev B* 2006, 73:045112.
33. Cai Y, Ke Q, Zhang G, Feng YP, Shenoy VB, Zhang YW. Giant phononic anisotropy and unusual an harmonicity of phosphorene: interlayer coupling and strain engineering. *Adv Funct Mater* 2015, 25:2230–2236.
34. Ong ZY, Cai Y, Zhang G, Zhang YW. Strong thermal transport anisotropy and strain modulation in single-layer phosphorene. *J Phys Chem C* 2014, 118:25272–25277.
35. Jain A, McGaughey AJH. Strongly anisotropic in-plane thermal transport in single-layer black phosphorene. *Sci Rep* 2015, 5:08501.
36. Li W, Carrete J, Mingo N. Thermal conductivity and phonon line widths of monolayer MoS_2 from first principles. *Appl Phys Lett* 2013, 103:253103.
37. Fei R, Faghaninia A, Soklaski R, Yan JA, Lo C, Yang L. Enhanced thermoelectric efficiency via orthogonal electrical and thermal conductances in phosphorene. *Nano Lett* 2014, 14:6393–6399.
38. Zhang S, Yang J, Xu R, Wang F, Li W, Ghufran M, Zhang YW, Yu Z, Zhang G, Qin Q, et al. Extraordinary photoluminescence and strong temperature/angle-dependent Raman responses in few-layer phosphorene. *ACS Nano* 2014, 8:9590–9596.
39. Wu J, Koon GKW, Xiang D, Han C, Tat Toh C, Kulkarni ES, Verzhbitskiy I, Carvalho A, Rodin AS, Koenig SP, et al. Colossal ultraviolet photo responsivity of few-layer black phosphorus. *ACS Nano* 2015, 9:8070–8077.
40. Peng X, Wei Q, Copple A. Strain-engineered direct–indirect band gap transition and its mechanism in two-dimensional phosphorene. *Phys Rev B* 2014, 90:085402.
41. Çakır D, Sahin H, Peeters FM. Tuning of the electronic and optical properties of single-layer black phosphorus by strain. *Phys Rev B* 2014, 90:205421.
42. Liu Q, Zhang X, Abdalla LB, Fazzio A, Zunger A. Switching a normal insulator into a topological insulator via electric field with application to phosphorene. *Nano Lett* 2015, 15:1222–1228.
43. Srivastava P, Hembram KPSS, Mizuseki H, Lee KR, Han SS, Kim S. Tuning the electronic and magnetic properties of phosphorene by vacancies and adatoms. *J Phys Chem C* 2015, 119:6530–6538.
44. Cai Y, Ke Q, Zhang G, Zhang YW. Energetics, charge transfer, and magnetism of small molecules physisorbed on phosphorene. *J Phys Chem C* 2015, 119:3102–3110.
45. Guo H, Lu N, Dai J, Wu X, Zeng XC. Phosphorene nanoribbons, phosphorus nanotubes, and van der Waals multilayers. *J Phys Chem C* 2014, 118:14051–14059.
46. Fei R, Yang L. Lattice vibrational modes and Raman scattering spectra of strained phosphorene. *Appl Phys Lett* 2014, 105:083120.
47. Fei R, Yang L. Strain-engineering the anisotropic electrical conductance of few-layer black phosphorus. *Nano Lett* 2014, 14:2884–2889.
48. Morgan Stewart H, Shevlin SA, Catlow CRA, Guo ZX. Compressive straining of bilayer phosphorene leads to extraordinary electron mobility at a new conduction band edge. *Nano Lett* 2015, 15:2006–2010.
49. Lu HY, Lu WJ, Shao DF, Sun YP. Enhanced thermoelectric performance of phosphorene by strain-induced band convergence. *Phys Rev B* 2014, 90:085433.
50. Kim J, Baik SS, Ryu SH, Sohn Y, Park S, Park B-G, Denlinger J, Yi Y, Choi HJ, Kim KS. Observation of tunable band gap and anisotropic Dirac semimetal state in black phosphorus. *Science* 2015, 349:723–726.
51. Pulizzi F. 2D materials: Semimetallic black phosphorus. *Nat Nanotechnol* 2015. doi:10.1038/nnano.2015.212.
52. Hu W, Yang J. Defects in phosphorene. *J Phys Chem C* 2015, 119:20474–20480.

53. Hu T, Hong J. First-principles study of metal adatom adsorption on black phosphorene. *J Phys Chem C* 2015, 119:8199–8207.
54. Hashmi A, Hong J. Transition metal doped phosphorene: first-principles study. *J Phys Chem C* 2015, 119:9198–9204.
55. Khan I, Hong J. Manipulation of magnetic state in phosphorene layer by non-magnetic impurity doping. *New J Phys* 2015, 17:023056.
56. Jing Y, Tang Q, He P, Zhou Z, Shen P. Small molecules make big differences: molecular doping effects on electronic and optical properties of phosphorene. *Nanotechnology* 2015, 26:095201.
57. Zhang R, Li B, Yang J. A first-principles study on electron donor and acceptor molecules adsorbed on phosphorene. *J Phys Chem C* 2015, 119:2871–2878.
58. Zhu Z, Li C, Yu W, Chang D, Sun Q, Jia Y. Magnetism of zigzag edge phosphorene nanoribbons. *Appl Phys Lett* 2014, 105:113105.
59. Li W, Zhang G, Zhang YW. Electronic properties of edge-hydrogenated phosphorene nanoribbons: a first-principles study. *J Phys Chem C* 2014, 118:22368–22372.
60. Han X, Stewart HM, Shevlin SA, Catlow CRA, Guo ZX. Strain and orientation modulated bandgaps and effective masses of phosphorene nanoribbons. *Nano Lett* 2014, 14:4607–4614.
61. Tran V, Yang L. Scaling laws for the band gap and optical response of phosphorene nanoribbons. *Phys Rev B* 2014, 89:245407.
62. Xia F, Wang H, Jia Y. Rediscovering black phosphorus as an anisotropic layered material for optoelectronics and electronics. *Nat Commun* 2014, 5:4458.
63. Radisavljevic B, Radenovic A, Brivio J, Giacometti V, Kis A. Single-layer MoS_2 transistors. *Nat Nanotechnol* 2011, 6:147–150.
64. Zhao S, Kang W, Xue J. The potential application of phosphorene as an anode material in Li-ion batteries. *J Mater Chem A* 2014, 2:19046–19052.
65. Li W, Yang Y, Zhang G, Zhang YW. Ultrafast and directional diffusion of lithium in phosphorene for high-performance lithium-ion battery. *Nano Lett* 2015, 15:1691–1697.
66. Uthaisar C, Barone V. Edge effects on the characteristics of Li diffusion in graphene. *Nano Lett* 2010, 10:2838–2842.
67. Li Y, Wu D, Zhou Z, Cabrera CR, Chen Z. Enhanced Li adsorption and diffusion on MoS_2 zigzag nanoribbons by edge effects: a computational study. *J Phys Chem Lett* 2012, 3:2221–2227.
68. Kulish VV, Malyi OI, Persson C, Wu P. Phosphorene as anode material for Na-ion batteries: a first-principles study. *Phys Chem Chem Phys* 2015, 17:13921–13928.
69. Sun J, Lee H-W, Pasta M, Yuan H, Zheng G, Sun Y, Li Y, Cui Y. A phosphorene–graphene hybrid material as a high-capacity anode for sodium-ion batteries. *Nat Nanotechnol* 2015. doi:10.1038/nnano.2015.194.
70. Zhu Z, Tománek D. Semiconducting layered blue phosphorus: a computational study. *Phys Rev Lett* 2014, 112:176802.
71. Boulfelfel SE, Seifert G, Grin Y, Leoni S. Squeezing lone pairs: the A17 to A7 pressure-induced phase transition in black phosphorus. *Phys Rev B* 2012, 85:014110.
72. Guan J, Zhu Z, Tománek D. Phase coexistence and metal-insulator transition in few-layer phosphorene: a computational study. *Phys Rev Lett* 2014, 113:046804.
73. Wu M, Fu H, Zhou L, Yao K, Zeng XC. Nine New Phosphorene polymorphs with non-honeycomb structures: a much extended family. *Nano Lett* 2015, 15:3557–3562.
74. Koenig SP, Doganov RA, Schmidt H, Castro Neto AH, Özyilmaz B. Electric field effect in ultrathin black phosphorus. *Appl Phys Lett* 2014, 104:103106.
75. Lu J, Wu J, Carvalho A, Ziletti A, Liu H, Tan J, Chen Y, Castro Neto AH, Özyilmaz B, Sow CH. Band gap engineering of phosphorene by laser oxidation towards functional 2D materials. *ACS Nano* 2015. doi:10.1021/acsnano.5b04623.
76. Dai J, Zeng XC. Structure and stability of two dimensional phosphorene with =O or =NH functionalization. *RSC Adv* 2014, 4:48017–48021.
77. Carvalho A, Castro Neto AH. Phosphorene: overcoming the oxidation barrier. *ACS Cent Sci* 2015, 1:289–291.
78. Deng Y, Luo Z, Conrad NJ, Liu H, Gong Y, Najmaei S, Ajayan PM, Lou J, Xu X, Ye PD. Black phosphorus–monolayer MoS_2 van der Waals heterojunction p–n diode. *ACS Nano* 2014, 8:8292–8299.
79. Cai Y, Zhang G, Zhang Y-W. Electronic properties of phosphorene/graphene and phosphorene/hexagonal boron nitride heterostructures. *J Phys Chem C* 2015, 119:13929–13936.
80. Avsar A, Vera-Marun IJ, Tan JY, Watanabe K, Taniguchi T, Castro Neto AH, Özyilmaz B. Air-stable transport in graphene-contacted, fully encapsulated ultrathin black phosphorus-based field-effect transistors. *ACS Nano* 2015, 9:4138–4145.
81. Sresht V, Pádua AAH, Blankschtein D. Liquid-phase exfoliation of phosphorene: design rules from molecular dynamics simulations. *ACS Nano* 2015, 9:8255–8268.

